11-1988

Transverse thermal velocity broadening of focused beams from liquid metal ion sources

J. W. Ward

R. L. Kubena

Mark Utlaut
University of Portland, utlaut@up.edu

Transverse thermal velocity broadening of focused beams from liquid metal ion sources

J. W. Ward, R. L. Kubena, and M. W. Utlaut[a)]
Hughes Research Laboratories, Malibu, California 90265

(Received 21 June 1988; accepted 24 August 1988)

Experiments have shown that the target current density in focused ion beam columns have long "tails" outside the central submicron region. We show that these tails result from a transverse velocity distribution which has a Holtsmark probability density. Both theory and experiment show that the tails are reduced as the system magnification and source current are reduced.

I. INTRODUCTION

Ion beam lithography using focused ion beams has emerged as one of the best techniques for the microfabrication of very high resolution structures.[1] Because of the much greater ion mass, scattering effects are much less important in determining the feature size and limiting pitch for ion beam lithography than for electron beam techniques. However, recent progress in reducing the spot size of focused ion beams and evidence for large tails[2–4] in their current–density distribution have led to increased interest in describing the parameters that limit feature size and packing density for focused ion beam lithography. In this paper, we describe the focusing limitations due to the transverse thermal velocity distribution of the emitted ions.

II. THERMAL VELOCITY EFFECTS

It is well known that thermal velocity effects are one of the principal limitations in the transport and focusing of high-density ion beams from conventional plasma-type ion sources. For example, Brewer[5] uses the theory worked out by Cutler and Hines[6] to show that for a Pierce geometry ion source having an emitter temperature of 1400 K and extraction potential of 10 kV, the mean deviation of a thermal velocity trajectory away from its laminar counterpart is ~ 7 μm at the beam minimum. This example shows that it is probably impossible to achieve a submicron spot with a conventional plasma-type ion source because of the effects of transverse thermal velocities.

The effects of transverse velocity on the spot size of a focused ion beam are shown schematically in Fig. 1. In this figure we show an ideal lens imaging a parallel beam into a focused spot at $M = 0$ or imaging a divergent beam from a point source into a focused spot at finite magnification M. In either case we show rays having a departure in slope of $\Delta r'$ from the laminar zero temperature trajectories due to the finite transverse ion temperature. For the parallel beam it can be easily shown that the spot growth r for a lens having focal length f is given by

$$r = f\,\Delta r'; \tag{1}$$

while for the finite magnification case with object distance d, it is given by[3]

$$r = Md\,\Delta r'. \tag{2}$$

To illustrate how these equations translate to an extreme sensitivity to transverse velocity consider a 50-kV Ga^+ beam ($u_\parallel \cong 3.7\times 10^5$ m/s). If we assume a transverse velocity of only 10 m/s, the corresponding slope error is $\Delta r' = u_\perp / u_\parallel \cong 3\times 10^{-5}$ rad. If we further assume a focal length of 2 cm (or a lens distance $d = 2$ cm with $M = 1$) then either equation predicts a radial spot growth of $r = (3\times 10^{-5})(2)\text{cm} = 0.6$ μm. Clearly, this example shows that the effects of transverse velocity are an important consideration in achieving submicron spot sizes.

In our first analysis[3] of the long tails which we had observed in our single-lens column we worked backward from the measured current density. We asked what distribution in ray height and slope in the aperture plane ~ 20 mm downstream of the emitter would produce the measured current density profiles. This study showed that the probability density function of the measured current density was a nearly exact replica of the transverse velocity distribution in the aperture plane. Not included in this approximation was the contribution from the ~ 0.1-μm-diam chromatic aberration disk in the very central region. Outside of this central region the spot radius is directly proportional to transverse velocity, so that the long tails in the current–density profile correspond to long tails in the transverse velocity distribution. This is illustrated in Fig. 2 where the probability density function for our single-lens column is plotted versus radius. Also shown in Fig. 2 is an equivalent transverse velocity scale converted from the radial position using Eq. (2) with

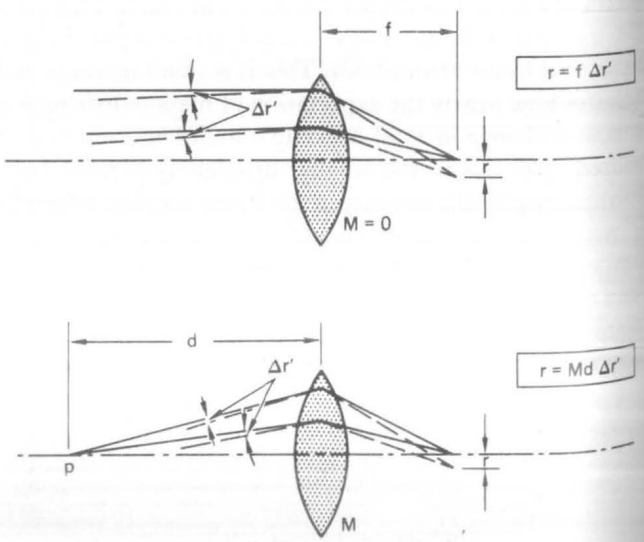

FIG. 1. Spot growth due to transverse velocity for parallel and divergent beams.

 0734-211X/88/062090-05$01.00

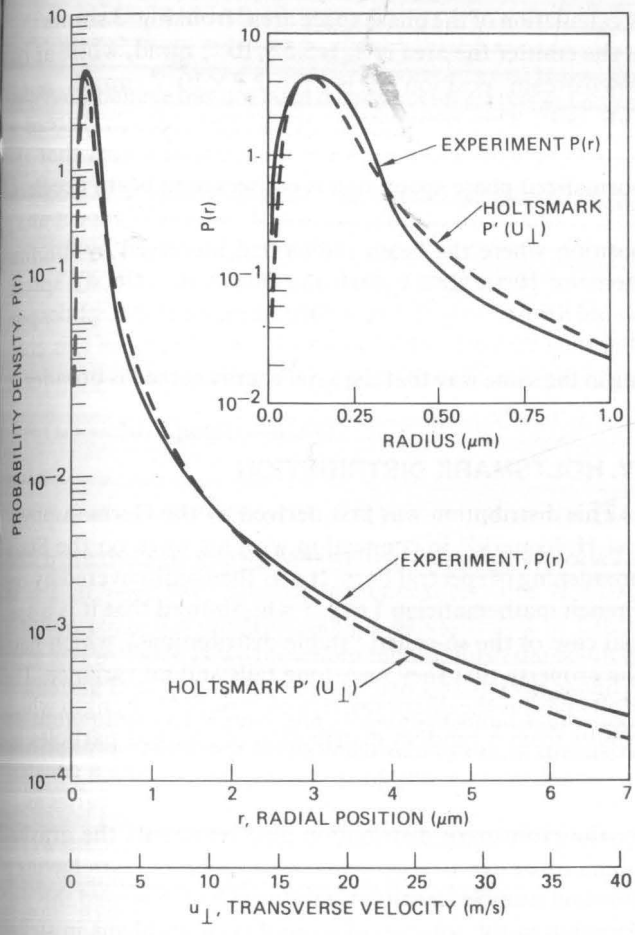

FIG. 2. Probability density function for target current density in single-lens column fitted with a Holtsmark distribution.

the single-lens values of $M = 1.04$ and $d = 20.8$ mm and a Ga^+ extraction voltage of 6.2 kV. Thus, a radius of 1 μm corresponds to a transverse velocity of ~ 6 m/s.

We have also plotted in Fig. 2 a curve scaled from the Holtsmark[14] distribution which is computed in Sec. IV. Note the excellent agreement between the experimental data and the Holtsmark distribution. We shall see in Sec. V that this agreement continues when we apply it to the more recent experimental data taken using our two-lens microprobe.

III. TRANSVERSE AND AXIAL VELOCITY SPREAD

As we have seen, one of the principal reasons for the "tails" on the current–density profiles is the transverse velocity distribution of the emitted ions. We will now discuss the effect of acceleration on an ion beam emitted with an initial temperature. Let us assume that the ions are emitted with a Maxwellian distribution of initial velocities in the x and y directions with zero mean and a variance equal to kT/m so that

$$\langle u_x^2 \rangle = kT/m \quad \text{and} \quad \langle u_y^2 \rangle = kT/m \,. \tag{3}$$

For the z direction we will assume a half-Maxwellian with the same temperature. We can also define temperature in terms of the full width at half-maximum (FWHM) of either the x or y velocity distribution so that

$$\text{FWHM} = 2.35\sqrt{kT/m} \,. \tag{4}$$

If we assume an initial root-mean-square Ga^+ velocity of ~ 1000 m/s the corresponding energy and temperature is ~ 0.72 eV and ~ 8400 K, respectively. When these ions are accelerated, the internal energy, as represented by the temperature, is reduced by a very large factor because a given velocity difference represents a much larger energy as the velocity increases. Zimmermann[8] has shown that the axial beam temperature in the moving frame is

$$kT_{\parallel} = (kT)^2/4eV_0 \tag{5}$$

and is extremely low after an acceleration of only a few kV. Using Eq. (5) for an initial temperature of 0.72 eV and an acceleration of $V_0 = 50$ keV we have

$$kT_{\parallel} = (0.72^2/4(50\,000) \cong 2.6 \times 10^{-6} \text{ eV} \,. \tag{6}$$

If we now solve for the mean-square velocity spread at this much lower temperature we find that $\langle u_z^2 \rangle^{1/2} \cong 1.9$ m/s. However, since energy differences are preserved in acceleration, the longitudinal energy spread remains at 0.72 eV. This large difference between energy spread and internal energy is tabulated in Table I as a function of mean-square velocity spread for both the axial and transverse directions. Zimmermann[8] and others have argued that since the transverse internal energy is not affected by the acceleration process the equipartition of energy will transfer this energy to the axial energy spread and will result in the anomalously high energy

TABLE I. Transverse and longitudinal energy spreads and temperatures for accelerated Ga^+ ion beam. $\delta u_z = u_z - \langle u_z \rangle$. $kT_{\parallel}/m = \langle \delta u_z^2 \rangle$; $kT_{\perp}/m = 1/2(\langle u_x^2 \rangle + \langle u_y^2 \rangle)$. $\Delta E_{\parallel} = 2\sqrt{kT_{\parallel} eV_0}$; $\Delta E_{\perp} = kT_{\perp}$.

Longitudinal temperature $\langle u_z \rangle \gg 0$		Longitudinal energy spread at $V_0 = 6$ kV	$V_0 = 60$ kV	Transverse temperature $\langle u_x \rangle = \langle u_y \rangle = 0$		Transverse energy spread at $r = r_0$	$r = gr_0$
$\langle \delta u_z^2 \rangle^{1/2}$ (m/s)	$kT_{\parallel}$ (eV)	$\Delta E_{\parallel}$ (eV)	$\Delta E_{\parallel}$ (eV)	$\langle u_x^2 \rangle^{1/2}$	$kT_{\perp}$	$\Delta E_{\perp}$	$\Delta E_{\perp}$
100	$\sim 0.72 \times 10^{-2}$	13.2	41.7	1000	~ 0.72	$kT_{\perp}$	$kT_{\perp}/g^2$
10	$\times 10^{-4}$	1.32	4.2	100	0.72×10^{-2}		
1	$\times 10^{-6}$	0.13	0.42	10	$\times 10^{-4}$		
				1	$\times 10^{-6}$		

spread first observed by Boersch and which has been verified by a number of experimenters. Other workers[16] have shown that the transverse temperature defined as

$$kT_\perp/m = (\langle \dot{x}^2 \rangle + \langle \dot{y}^2 \rangle)/2 \tag{7}$$

varies as $T_\perp r^2 = \text{const}$ so that we would expect a large drop in transverse internal energy as ions are accelerated away from the emitter in a liquid metal ion source where there is considerable expansion in the radial direction. To investigate this further we computed trajectories in a sphere-on-orthogonal [18](SOC) diode using our Monte Carlo[13] computer program. Figure 3 shows the large reduction in transverse velocity which occurs after the ions are accelerated only a short distance downstream of the SOC emitter. The initial conditions assumed for this calculation were

$$\langle \dot{x}^2 \rangle = \langle \dot{y} \rangle^2 = \langle \dot{z}^2 \rangle = kT/m \quad \text{for} \quad kT = 1.4\ \text{eV}. \tag{8}$$

Note that the transverse velocity has been reduced from an initial spread of $\sim \pm 2000$ m/s to a spread of $\sim \pm 110$ m/s.

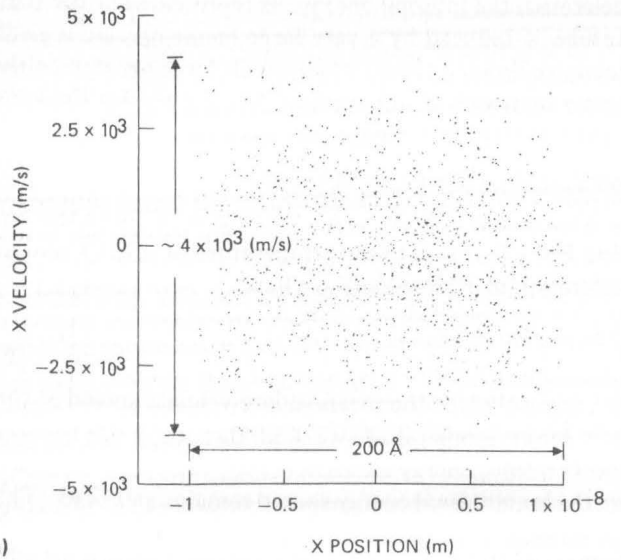

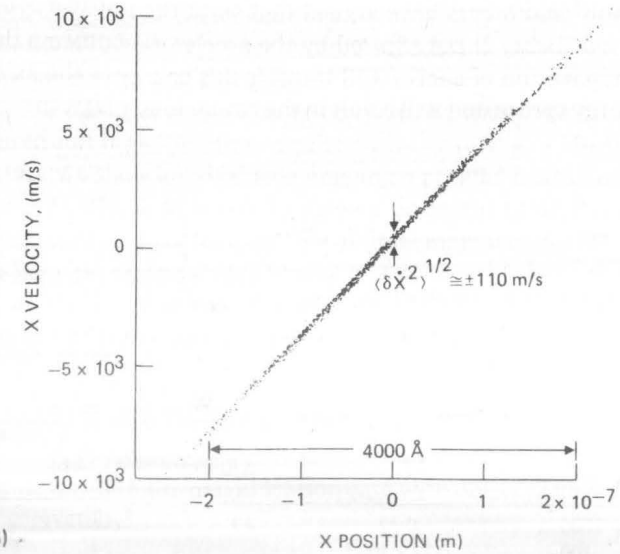

FIG. 3. Computer simulation of beam cooling in a SOC diode due to large radial expansion: (a) at emitter, $V(z) = 0$, initial temperature 1.4 eV; (b) 1 μm downstream of emitter, $V(z) \cong 808$.

A calculation of the phase space area[3] from Fig. 3 shows that at the emitter the area is $A_0 \cong 5.5 \times 10^{-8}$ mrad, while at the downstream position it is $A_1 \cong 2.3 \times 10^{-9}$ mrad $\cong A_0/\sqrt{eV_1/kT}$. This reduction in transverse velocity spread is consistent with Liouville's theorem which states that the normalized phase space area is conserved in beam acceleration. If this beam cooling continued, we might expect at a z position where the beam radius had increased by another factor of 10 (at $2r \cong 4$ μm), the transverse velocity spread would drop to $\sim \pm 1.1$ m/s. Of course, we also might expect that the Coulomb collisions would cancel some of this cooling in the same way that the axial energy spread is broadened after emission.

IV. HOLTSMARK DISTRIBUTION

This distribution was first derived by the German physicist Holtsmark[14] in connection with his work on the Stark broadening of spectral lines. It was then rediscovered by the French mathematician Levy,[15] who showed that it is a special case of the so-called "stable distributions" which have the property that they have long tails and no variance. The Holtsmark is the distribution in electric field strength which results from a random distribution of charged particles interacting with a Coulomb $1/r^2$ force and having a constant charge density. Since the gravitational force also varies as $1/r^2$, the Holtsmark distribution also represents the gravitational force due to a random distribution of stars having a constant number density. Chandrasekhar[7] has used this distribution in the solution of a number of problems in stellar dynamics. Because we found no tables for the two-dimensional Holtsmark in the literature, we now describe how we numerically evaluated the Holtsmark in all three dimensions. We believe our calculations are accurate to at least four significant figures. The tables for the Holtsmark distribution given in Refs. 7 and 9 have only one significant figure for large values of the argument.

It can be shown that the characteristic function of the stable distribution is[10]

$$\exp[-\sigma^2/2|k|^\beta] \quad 0 < \beta \leqslant 2, \tag{9}$$

where the parameter σ^2 plays the role of the variance although the second moment (variance) is never finite for $\beta < 2$. Expressing the probability distribution for the velocity $\bar{u}$ as the Fourier transform of the characteristic function we have for $n = 1$, 2, and 3 dimensions and putting $\sigma^2 = 2$ we have that

$$P(\bar{u}) = \frac{1}{(2\pi)^n} \int_{-\infty}^{\infty} \exp(-|\bar{k}|^\beta) \exp(-i\bar{k}\cdot\bar{u})\, d\bar{k}, \tag{10}$$

where the integral is evaluated over the entire range of the n-dimensional vectors $\bar{u}$ and $\bar{k}$. For the Holtsmark, the characteristic exponent, beta, is $\frac{3}{2}$ while the Gaussian and Cauchy distributions are obtained as special cases when $\beta = 2$ and 1.

From Eq. (10) we obtain for $n = 3$, following the same steps outlined by Chandrasekhar[7] where $|u| = (u_x^2 + u_y^2 + u_z^2)^{1/2}$, that

$$P_3(|u|) = \frac{2|u|}{\pi} \int_0^{\infty} \exp(-k^\beta) k \sin(k|u|)\, dk. \tag{11}$$

For $n = 2$ where $|u| = (u_x^2 + u_y^2)^{1/2}$, we find

$$P_2(|u|) = |u| \int_0^\infty \exp(-k^\beta) k J_0(k|u|) dk, \qquad (12)$$

which we believe has not been derived before. Here $J_0(k|u|)$ is the zero-order Bessel function. For $n = 1$ it is easy to show that Eq. (10) reduces to

$$P_1(u) = \frac{1}{\pi} \int_0^\infty \exp(-k^\beta) \cos(ku) dk, \qquad (13)$$

since $P_1(u)$ is an even function in the one-dimensional case. As a check we evaluated Eqs. (11)–(13) for $\beta = 2$ (Gaussian) and obtained

$$P_1(u) = (1/2\sqrt{\pi}) \exp(-u^2/4),$$

$$P_2(u) = (u/2) \exp(-u^2/4),$$

and

$$P_3(u) = (u^2/2\sqrt{\pi}) \exp(-u^2/4), \qquad (14)$$

which are the well-known Maxwellian distributions for $kT/m = 2$ in one, two, and three dimensions. For $\beta = 3/2$ (Holtsmark), the integrals cannot be expressed in closed form and in Table II we present in tabular form the result of evaluating Eqs. (11)–(13) for $u = 0$ to 100. In Figs. 4 and 5, we show plots of the one- and two-dimensional Holtsmark distributions. Note that in the linear plot of Fig. 4, the distributions are nearly identical out to about $u = 5$. However, we see in the log plot of Fig. 5 that slightly past this value, the Maxwellian is dropping very rapidly compared to the Holtsmark. Mandelbrot[11] has called this slow drop-off in the tail region "hyperbolic" and shows that for the Holtsmark distribution, the probability in the tail region varies as $P(u) \propto u^{-5/2}$. This slow drop-off results in an infinite variance $\langle u^2 \rangle = \infty$, so there is no characteristic size for any of the stable distributions which have $\beta < 2$. He also shows that this absence of characteristic size is one of the features of self-similarity or scale invariance which is also one of the most important features of fractals.[17]

TABLE II. The Holtsmark distribution in one, two, and three dimensions for $\sigma^2 = 2$.

u	$P_1(u)$	$P_2(u)$	$P_3(u)$
0.00	2.8735E − 01	0.0000E + 00	0.0000E + 00
0.20	2.8315E − 01	1.1710E − 01	1.6665E − 02
0.40	2.7099E − 01	2.2336E − 01	6.3088E − 02
0.60	2.5215E − 01	3.0759E − 01	1.2959E − 01
0.80	2.2847E − 01	3.6614E − 01	2.0323E − 01
1.00	2.0204E − 01	3.9701E − 01	2.7122E − 01
1.20	1.7485E − 01	4.0262E − 01	3.2378E − 01
1.40	1.4855E − 01	3.8794E − 01	3.5570E − 01
1.60	1.2434E − 01	3.5910E − 01	3.6633E − 01
1.80	1.0292E − 01	3.2211E − 01	3.5850E − 01
2.00	8.4540E − 02	2.8201E − 01	3.3694E − 01
4.00	1.3673E − 02	5.4173E − 02	8.0674E − 02
6.00	4.2235E − 03	1.6203E − 02	2.3822E − 02
8.00	1.9065E − 03	7.1502E − 03	1.0350E − 02
10.00	1.0478E − 03	3.8629E − 03	5.5614E − 03
20.00	1.7337E − 04	6.3037E − 04	8.8558E − 04
40.00	2.9944E − 05	1.0807E − 04	1.5086E − 04
60.00	1.0803E − 05	3.8922E − 05	5.4241E − 05
80.00	5.2512E − 06	1.8900E − 05	2.6321E − 05
100.00	3.0016E − 06	1.0801E − 05	1.5037E − 05

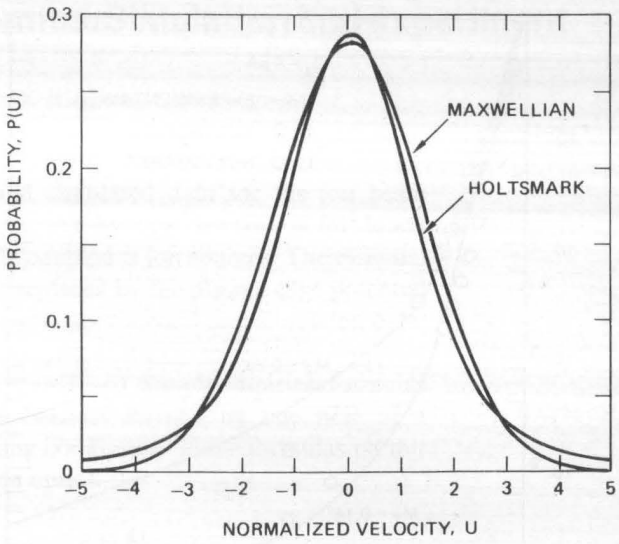

FIG. 4. One-dimensional Maxwellian and Holtsmark velocity distributions for $\sigma^2 = 2$.

V. CALCULATION OF TARGET CURRENT DENSITY

Figure 6 shows Ga^+ target current–density profiles measured at two different magnifications on our 50-keV, two-lens ion microprobe system. A complete description of the experimental conditions and the measurement technique using dot exposures of bilevel negative resist is given in Ref. 2. We see that these profiles have long tails extending out to several thousand angstroms at 10^{-5} of the peak density. We will now describe the computer model used to simulate these beam profiles. The basic idea is that the current density at the target is determined by the combination of effects due to the virtual source (transverse velocity spread) plus the effects due to the chromatic aberration of lenses (longitudinal ve-

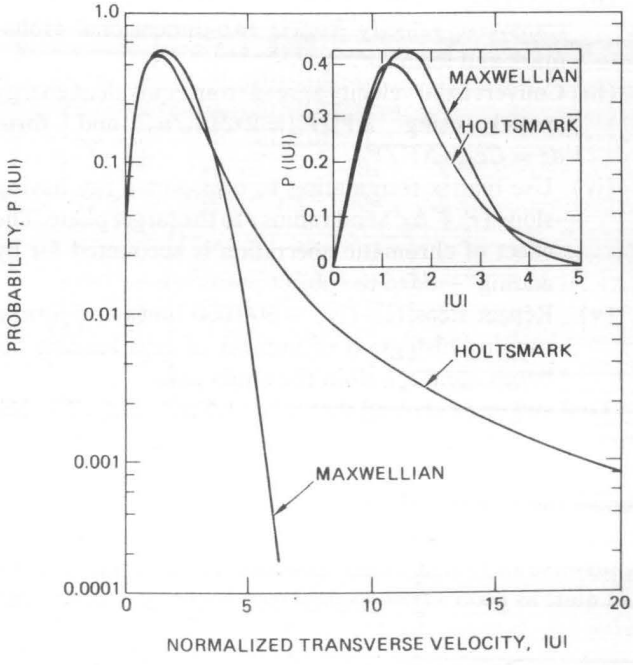

FIG. 5. Two-dimensional Maxwellian and Holtsmark distributions for $\sigma^2 = 2$.

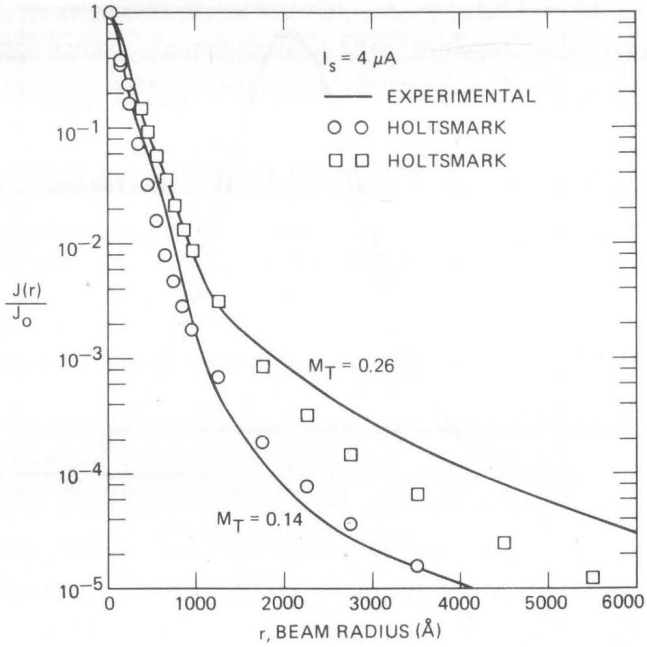

FIG. 6. Current–density profiles of the 50-keV Ga^+ ion microprobe vs system magnification for experimental and from simulation using Holtsmark distribution.

locity spread). This model has only two adjustable parameters which are the FWHM widths of the transverse and longitudinal (Holtsmark) velocity distributions measured in the aperture plane. The details of the mapping process are more fully described in Ref. 3 so we will briefly describe the computer simulations.

(i) Choose three random numbers from the one-dimensional Holtsmark distribution. The first two δu_x and δu_y are from a distribution having width $w1$ and the third $\delta u_{\|}$ is from a distribution with width $w2$.

(ii) Form $\delta u_{\perp} = \sqrt{\delta u_x^2 + \delta u_y^2}$ which represents a random transverse velocity from a two-dimensional Holtsmark and form $\Delta r'$.

(iii) Convert axial velocity spread to an equivalent energy spread using $\Delta V/V_0 = 2*\delta u_{11}/u_0$ and form $dz = Cc_{0b}*\Delta V/V_0$.

(iv) Use matrix formulation to transport a ray having slope $(r' + \Delta r')$ and radius r to the target plane. The effect of chromatic aberration is accounted for by adding $\pm dz$ to the object positions.

(v) Repeat steps (i)–(iv) ~300 000 times and form a running histogram of number of rays landing between r and $r + dr$ in the target plane.

Trial and error showed that $w1 = 1.5$ m/s and $w2 = 160$ m/s accurately represent the $M = 0.14$ data in Fig. 6. We next changed the matrix coefficients of the second lens to model the longer working distance for the $M = 0.26$ case. We then reran the simulation using the same "seed" for the transverse and longitudinal velocities. The new simulation is not quite as good as the original, but is still quite good especially for the smaller radii. If we convert the FWHM Holtsmark values to an equivalent root-mean-square velocity using Eq. (4) (which rigorously only applies to a Maxwellian), we find that the widths $w1$ and $w2$ become $\langle u_x^2\rangle^{1/2} = \langle u_y^2\rangle^{1/2} = 1.5/2.35 \cong 0.64$ m/s and $\langle u_z^2\rangle^{1/2} = 160/2.35 \cong 68$ m/s equivalent root-mean-square velocities. Converting these values to equivalent temperatures using Eq. (3), we see that $kT_{\perp} \simeq 6\times10^{-7}$ eV and $kT_{\|} = 3.3\times10^{-3}$ eV. Using Eq. (5) to convert this longitudinal temperature to an equivalent energy spread we have that $\Delta E_{\|} = 2\sqrt{(3\times10^{-3})^2 6200} \cong 9$ eV. This is not too far from the 8-eV value that was reported in Ref. 12 for a 4-μA Ga^+ source current. We also see that the large difference between the transverse and longitudinal temperature implies that there is negligible exchange of energy between the transverse and longitudinal directions.

VI. CONCLUSIONS

Experiments have shown that the target current density in focused ion beam columns have long tails outside the central submicron region. We have shown that these tails result from a transverse and longitudinal velocity distribution which has a Holtsmark probability distribution. We have described a computer model used to accurately simulate the measured current–density profiles. This model has only two adjustable parameters which are the FWHM widths of the transverse and longitudinal velocity distributions. Both theory and experiment show that the long tails are reduced as the system magnification and extracted source currents are reduced.

[a] Present address: University of Portland, 5200 N. Willamette Boulevard Portland, OR 97203.

[1] R. L. Kubena, R. J. Joyce, J. W. Ward, H. L. Garvin, F. P. Stratton, and R. G. Brault, Appl. Phys. Lett. **50**, 1589 (1987).
[2] R. L. Kubena and J. W. Ward, Appl. Phys. Lett. **51**, 1960 (1987).
[3] J. W. Ward, M. W. Utlaut, and R. L. Kubena, J. Vac. Sci. Technol. B **5**, 169 (1987).
[4] Y. Kawanami, T. Ishitani, K. Umemura, and S. Shukuri, J. Vac. Sci. Technol. B **5**, 1364 (1987).
[5] R. Wilson and G. Brewer, *Ion Beams* (Krieger, New York, 1979), p. 145.
[6] C. C. Cutler and M. E. Hines, Proc. IRE **43**, 307 (1955).
[7] S. Chandrasekhar, Rev. Mod. Phys. **15**, 1 (1943).
[8] B. Zimmermann, Adv. Electron. Electron Phys. **29**, 257 (1970).
[9] D. R. Holt and E. L. Crow, J. Res. Natl. Bur Stand. **778** (3/4), 143 (1973).
[10] J. L. Doob, Ann. Math. **43**, 351 (1942).
[11] B. B. Mandelbrot, *The Fractal Geometry of Nature* (Freeman, New York, 1983), p. 372.
[12] A. E. Bell and L. W. Swanson, Appl. Phys. A **41**, 335 (1986).
[13] J. W. Ward, J. Vac. Sci. Technol. B **3**, 207 (1985).
[14] J. Holtsmark, Ann. Phys. **58**, 577 (1919).
[15] P. Lévy, *Calcul des Probabilities* (Gautheir–Villars, Paris, 1925), Part II, Chap. 6.
[16] H. Rose and R. Spehr, in *Advances in Electronic and Electron Physics*, edited by A. Septier (Academic, New York, 1983), Suppl. C, p. 473.
[17] H. Takayasu, Prog. Theor. Phys. **72**, 471 (1984).
[18] W. Dyke and W. Dolan, *Advances in Electronics and Electron Physics* (Academic, New York, 1956), p. 90.